Dual Thermo- and pH-Responsive N -Cyanomethylacrylamide-Based Nano-Objects Prepared by RAFT-Mediated Aqueous Polymerization-Induced Self-Assembly

Nicolas Audureau, Fanny Coumes, Jean-Michel Guigner, Clément Guibert, François Stoffelbach, Jutta Rieger

Dual thermo- and pH-responsive *N*-cyanomethylacrylamide-based nano-objects prepared by RAFT-mediated aqueous PISA

Nicolas Audureau[1], Fanny Coumes[1], Jean-Michel Guigner[2], Clément Guibert[3], François Stoffelbach[1]*, Jutta Rieger[1]*

[1] Sorbonne Université & CNRS, UMR 8232, Institut Parisien de Chimie Moléculaire (IPCM), Polymer Chemistry Team, 4 Place Jussieu, 75252 Paris Cedex 05, France

[2] Sorbonne Université & CNRS, UMR 7590, Institut de Minéralogie, de Physique des Matériaux et de Cosmochimie (IMPMC)-IRD-MNHN, 75252 Paris Cedex 05, France

[3] Sorbonne Université & CNRS, UMR 7197, Laboratoire de Réactivité de Surface (LRS), 4 Place Jussieu, 75252 Paris Cedex 05, France

francois.stoffelbach@sorbonne-universite.fr; jutta.rieger@sorbonne-universite.fr

Graphical abstract

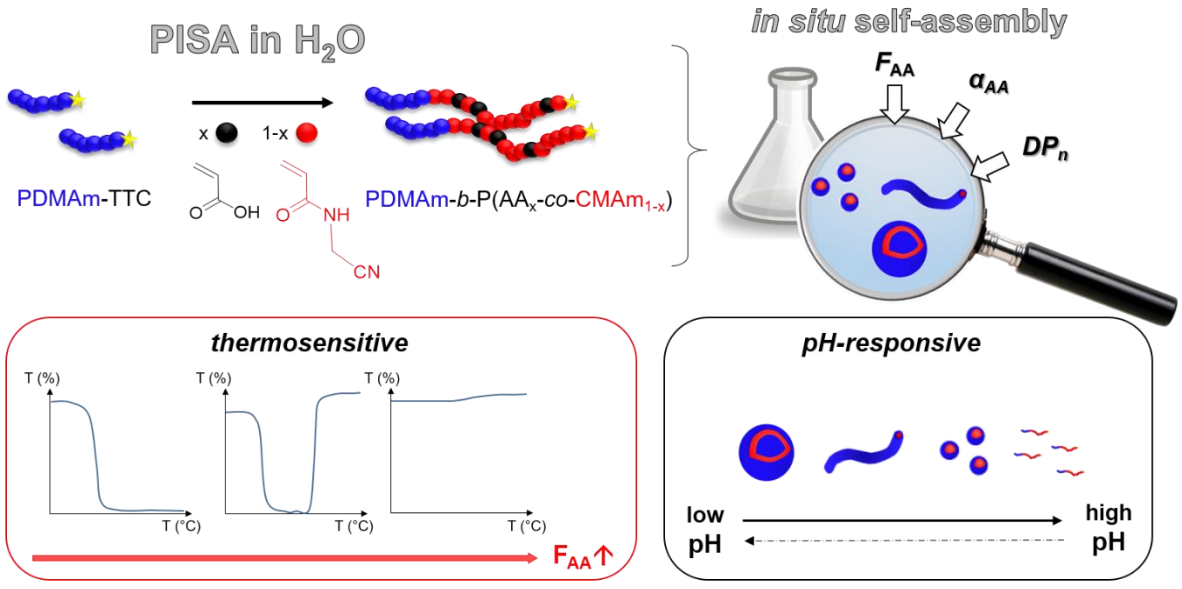

Abstract

We report the straightforward synthesis of dual stimuli-responsive nano-objects using a RAFT-mediated polymerization-induced self-assembly (PISA) process in water. The key to complex and tunable responsiveness was the copolymerization of *N*-cyanomethylacrylamide, providing UCST-type polymers, with a pH-sensitive monomer (acrylic acid, AA). Not only the core block length, but also the acrylic acid content and slight changes in the degree of ionization of AA in the polymerization medium ($\alpha_{AA,0}$) had a great impact on the particle morphology. Generally, higher AA contents favored the formation of spherical nano-objects, while low $\alpha_{AA,0}$ led to higher order morphologies. We demonstrated that the nano-objects exhibited a complex dual responsiveness to changes in the degree of ionization and temperature. Progressively increasing post-polymerization the degree of ionization of the AA units incorporated in the copolymer (α_{AA}) triggered morphological transitions. Remarkably, a single copolymer composition formed well-defined vesicles, worms, and spheres that eventually dissociated into individual chains. Temperature-dependent SAXS analyses evidenced a complex thermo-responsive behavior, which depended on the copolymer composition and α_{AA}. For some compositions, we observed both a cloud and a clearing point, attributed to the formation of secondary aggregates and chain dissolution, respectively.

1. Introduction

Over the last decade, polymerization-induced self-assembly (PISA) has emerged as a powerful and straightforward technology for the rational design of block copolymer nano-objects.[1–5] In essence, PISA relies on the chain extension of a soluble precursor block with an insoluble second block in a selective solvent, such as water. Simultaneously to its production, the amphiphilic diblock self-assembles into nano-objects with various shapes, such as spheres,

worms or vesicles. Numerous polymers have been studied, varying for instance in hydrophobicity, glass transition temperature (T_g) or exhibiting functional properties. Recent developments target the design of reactive and functional nanoparticles,[6,7] which paves the way to new applications. Therefore, stimuli-responsive nanoparticles that exhibit response to changes in temperature[8–15], pH-[16] or reactive additives[17–19] have been developed. Whereas the stimuli-induced dissolution of nano-objects has often been reported in the literature for nano-assemblies prepared post-polymerization (by classical methods, such as nanoprecipitation), their stimuli-induced morphological transitions have rarely been reported. In contrast, there are a few reports demonstrating that PISA-derived nanoparticles are able to change morphology as a function of temperature.[8–14] The observed morphological transitions, mainly sphere-to-worm-(to-vesicle) order-order transitions, have been explained by subtle changes in the degree of (partial) hydration of the core-forming block,[11,13,20] most of them relying on a lower critical solution temperature (LCST)-type core dehydration occurring upon heating. We have recently shown that the use of upper critical solution temperature (UCST)-type polymers as core block allows to induce reverse transitions (worm-to-sphere transition upon heating).[15] Moreover, an impact of the polymerization temperature during PISA on particle morphology has also been mentioned in the literature.[21,22] Concerning pH-induced morphological transitions, there are less examples in the literature. Remarkably, it has been demonstrated that pH-responsive monomer units in the shell block[3,23] or the presence of a single terminal carboxylic acid or amino group[16,24,25] were able to induce, post-polymerization, order-order morphological transitions, *via* pH variation of the medium. The transitions were explained by modification of the packing parameter as a response to ionization of the pH-sensitive unit(s). There is less literature on the insertion of a pH-responsive comonomer into the core block. Hong *et al.*[26] synthesized diblock copolymers containing a pH-sensitive comonomer [(diisopropylamino)ethyl methacrylate, DIPEMA, with a pK_a = 6.3] in the hydrophobic block

by PISA. They evidenced a complete dissolution of their vesicles when the pH was reduced resulting in the protonation of the DIPEMA units, but no morphological transitions. Remarkably, it was recently reported that a single composition of amphiphilic diblock copolymer comprising acrylic acid (AA) units in both blocks (16 mol% and 84 mol% AA content, respectively) was able to form spheres, worms and vesicles depending on the solution pH.[27] However, to obtain the desired copolymer composition, the copolymer was produced in solution through a sequential reagent addition protocol, using an automated parallel synthesizer.

In this project, we report a straightforward method to produce nano-objects that exhibit a complex and tunable dual response to two stimuli, namely temperature and pH. We chose poly(*N*-cyanomethylacrylamide) (PCMAm) as a core-forming block, as we had previously demonstrated that PCMAm exhibits a UCST-like temperature transition in water.[28] UCST-polymers have only rarely been combined with PISA,[12,15,29] although they are of great interest in particular for the development of biomaterials.[30–35] In comparison to the well-studied poly(acrylamide-*co*-acrylonitrile) (P(Am-*co*-AN)),[15,29,36–39] which requires the handling of the volatile and toxic AN, the polymerization of CMAm (a solid) stands out by its straightforward synthesis. In a previous work, we demonstrated that it was possible to extend a hydrophilic poly(*N*,*N*-dimethylacrylamide) (PDMAm) macroRAFT agent with a PCMAm block via a RAFT-mediated PISA process with good polymerization control. Depending on the DP_n, various morphologies, namely spheres, worms and vesicles, could be formed.[12] Only distinct compositions (with a short PCMAm block, $DP_{n,PCMAm} < 100$) exhibited a thermo-responsive behavior with a clearing point. No morphological transitions were observed. The lack of thermoresponsiveness for higher $DP_{n,PCMAm}$ was attributed to a too high transition temperature (above 90 °C), which might be remediated by the copolymerization of CMAm with hydrophilic comonomers.[28]

The aim of this study was to synthesize nano-objects by PISA, whose morphology and assembly can be controlled by two stimuli, namely temperature and pH, through the ionization of a pH-sensitive comonomer inserted in the solvophobic block. For that purpose, AA was introduced as a comonomer in the polymerization of CMAm. We postulated that PDMAm-*b*-P(CMAm-*co*-AA) diblock copolymers might display morphological transition upon pH change. Furthermore, we expected that these diblocks could molecularly dissolve in case the AA units are present in sufficient amount, and sufficiently ionized. The impact of the molar fraction of AA and its degree of ionization (α_{AA}) on morphology was studied both during PISA, or post-polymerization. Finally, their thermoresponsiveness was investigated by turbidity measurements, cryo-transmission electron microscopy (cryo-TEM), dynamic light scattering (DLS), and small-angle X-ray scattering (SAXS) experiments.

2. Experimental section

2.1. Materials

N-Cyanomethylacrylamide and ethyl 2-(butylthiocarbonothioylthio) propanoate (CTA1) were synthesized according to protocols previously described.[28] 2,2′-Azobis(isobutyronitrile) (AIBN, ≥ 98%, Aldrich), 2,2'-azobis[2-(2-imidazolin-2-yl)propane]dihydrochloride (VA-044) (Aldrich, 98%), 1,3,5-trioxane (Aldrich, ≥ 99%), acrylic acid (AA) (Aldrich, 99%) and *N*,*N*-dimethylformamide (DMF, VWR, Normapur) were used as received. *N*,*N*-Dimethylacrylamide (DMAm) (Aldrich, ≥ 99%) was distilled under reduced pressure before use. Deionized water was used for the aqueous polymerizations. PDMAm macroRAFT (DP_n = 36) (PDMAm$_{36}$-TTC) and PDMAm$_{36}$-*b*-PCMAm$_{186}$ diblock copolymers, used for comparison, were synthesized as described before.[12]

2.2. Synthesis of PDMAm-*b*-P(CMAm-*co*-AA) diblock copolymers in water

In a typical experiment (Entry 3, **Table 1**), 53 mg (0.014 mmol) of $PDMAm_{36}$-TTC, 100 µL of an initiator solution (11.8 mg of VA-044 (2,2'-azobis[2-(2-imidazolin-2-yl) propane]dihydrochloride) diluted in 1.01 g of deionized water) (0.004 mmol) and 259 mg (2.35 mmol) of CMAm were dissolved in 2.9 g of water in a 10 mL septum-sealed round bottom flask. The mixture was purged with argon for 30 min in a cold-water bath. 0.025 mL (0.36 mmol) of degazed AA is introduced via an air-tight syringe in the flask. The flask was immersed in a thermostated oil bath at 45 °C for 4.6 h. Monomer conversion was kinetically followed by taking aliquots from the reaction media and analyzing them by ^{1}H NMR. The polymerization was quenched by exposure to air and placing the flask into an ice bath. Stable polymer dispersion in water was obtained. Unlike experiments *1* to *4*, the polymerizations of *samples 5, 6* and 7 were performed in 0.03M HCl, whereas the polymerization of *sample 8* was performed in 0.06M NaOH aqueous solution.

2.3. Characterization techniques

NMR spectroscopy

^{1}H NMR spectra were recorded in DMSO-d_6 (unless stated differently) at 300 K on a Bruker 300 MHz spectrometer in 5-mm diameter tubes.

Size exclusion chromatography (SEC)

SEC measurements were carried out at 60 °C in DMF (+ LiBr, 1g L^{-1}) as mobile phase at a flow rate of 0.8 mL min^{-1} and with toluene as a flow rate marker. All polymers were prepared at a concentration ranging from 5 to 10 mg mL^{-1} then filtered through a 0.20 µm PTFE membrane; 100 µL of ready solution was injected for each measurement for analysis. The

separation system was composed of two PSS GRAM 1000 Å columns (8 x 300 mm; separation limits: 1 to 1000 kg mol^{-1}) and one PSS GRAM 30 Å (8 x 300 mm; separation limits: 0.1 to 10 kg mol^{-1}) coupled with a modular differential refractive index (RI) detector Viscotek 3580. Molar masses (M_n, the number-average molar mass, M_w, the weight-average molar mass) and dispersities ($Đ = M_w/M_n$) were calculated using OmniSEC 5.12 software with a calibration curve based on narrow PMMA standards (M_p range: 981 000 to 625 g mol^{-1}) from Polymer Standard Services.

Turbidimetry

Turbidimetry measurements of copolymers in water were performed on an Agilent spectrophotometer Cary 100 UV-Vis equipped with a Peltier-type temperature control system by measuring the transmittance at a wavelength of 670 nm. The heating/cooling rate was maintained constant at 1 °C min^{-1}. Samples were prepared at a concentration of 1 wt% by diluting the polymer dispersion in ultra-pure water (unless stated differently). All measurements were performed with deionized water (unless stated differently). The cloud point and clearing point (T_{CP}) were determined at the inflection point.

Dynamic Light Scattering analyses (DLS)

Dynamic Light Scattering (DLS) measurements were carried out on a Zetasizer Nano S90 from Malvern (90° angle, 5 mW He–Ne laser at 633 nm) to determine the z-average particle diameter (D_z) of diluted dispersions in water at 0.1 wt% concentration (unless stated differently). The polydispersity index (PDI) was determined with the cumulant method.

pH-measurements

pH measurements were realized with a Mettler Toledo DL50 Graphix pH meter connected with an InLab Micro electrode.

Cryo-TEM

Cryogenic Transmission Electron Microscopy (cryo-TEM) analyses: polymer solution was prepared at 1 wt% in ultra-pure water (unless otherwise stated). 3 µL of the solution was then deposited on a quantifoil grid. After removing the excess of solution with a Whatman paper, the grid was immediately frozen in liquid ethane. The observations were carried out at -180 °C by a JEOL JEM-2100 LaB_6 microscope operating at 200 kV. The images were taken on a Gatan US 1000, 2k by 2k CCD Camera. For samples for which alpha was varied post-polymerization, the dispersions were diluted 3-4 days prior the analysis to allow a good equilibrium (unless stated differently).

Small Angle X-ray Scattering analyses (SAXS)

Small angle X-ray Scattering Analyses (SAXS). Selected samples were analyzed by small angle X-ray scattering (SAXS) measurements on the SWING beamline of the SOLEIL Synchrotron (Saint Aubin, France). The measurements were performed in two series of measurements at an energy of 7 keV (λ = 1.77 Å) and 12 keV (λ = 1.03 Å), with an exposure time of 1000 ms and a gap time of 500 ms and measured by a two-dimensional CCD detector (EigerX4M in vacuum, 162.5 × 155.2 mm², pixel size : 75 × 75 µm²) localized at a distance of 2131 mm (or 3500 mm) from the sample corresponding to a q-range of 1.7×10^{-3} to 0.31 $Å^{-1}$ (or 1.8×10^{-3} to 0.32 $Å^{-1}$). The measurements were performed at different temperatures thanks to a thermostated capillary-holder device at a concentration of 1 wt%. At this concentration, interparticle interactions are negligible.[12] Standard correction procedures were applied for X-

ray beam transmission, detector efficiency and signal subtraction of the 1.5 mm capillary filled with the solvent. The softwares *Foxtrot*® and SaSview were used to achieve such data reduction. The SAXS measurements were performed at different temperatures thanks to a thermostated capillary-holder device, the targeted temperature being maintained for 3 to 5 min prior to measurements. The data was fitted with the SasView software (http://www.sasview.org/). According to the observed morphologies using cryo-TEM, the data were fitted with the form factor of a lognormal distribution of either spheres, cylinder or vesicles.[40–42]

3. Results and discussion

In order to confer pH-sensitive properties to the previously discussed PDMAm-*b*-PCMAm system[12], we inserted acrylic acid monomer units into the hydrophobic PCMAm block.

Synthesis of PDMAm-b-P(CMAm-co-AA) diblock copolymers

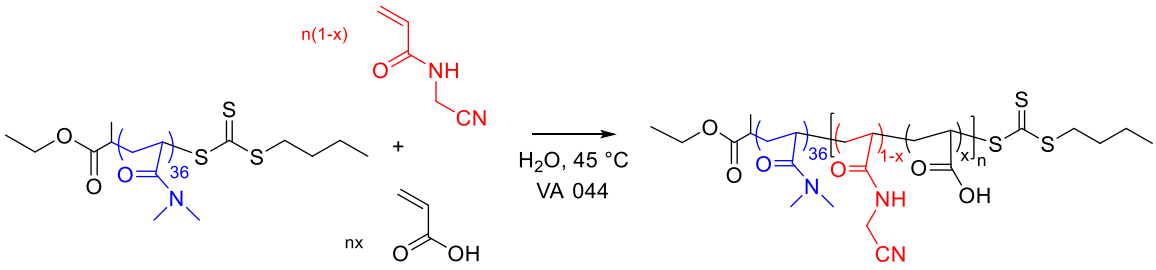

Scheme 1. Synthesis route employed in this study for the preparation of pH-responsive nano-assemblies.

As summarized in Scheme 1, the synthesis strategy relied on the aqueous RAFT copolymerization of CMAm and AA in the presence of a trithiocarbonate (TTC) PDMAm macromolecular RAFT agent (macroRAFT agent) used as a reversible chain transfer agent (CTA) to promote the formation of amphiphilic diblock copolymers. In the case where an

insoluble P(CMAm-*co*-AA) block is formed during synthesis, the polymerization mechanism is a dispersion polymerization, and PDMAm-*b*-P(CMAm-*co*-AA) diblock copolymer nanometric assemblies should be formed according to the polymerization-induced self-assembly (PISA) strategy.

3.1. Statistical copolymerization of CMAm with AA in the presence of a $PDMAm_{36}$ macroRAFT agent

In our previous work on PDMAm-*b*-PCMAm[12], we showed that a long PDMAm stabilizer was necessary to guarantee a good colloidal stability of the PDMAm-*b*-PCMAm self-assemblies formed *via* PISA, and we therefore selected a PDMAm stabilizer with DP_n = 36 ($PDMAm_{36}$-TTC) as a macroRAFT agent (Table S1 and Figure S1) to synthesize PDMAm-*b*-P(CMAm-*co*-AA) diblock copolymers *via* aqueous RAFT copolymerization. The copolymerization of CMAm with AA was performed at 10 wt% at 45 °C, *i.e.* using the reported conditions.[12] The initial monomer/CTA molar ratio was kept constant at 200.

Table 1. Experimental conditions and results for aqueous copolymerizations of AA and CMAm in the presence of $PDMAm_{36}$ macroRAFT agent[#]

Entry	Solvent of polymerization	$\alpha_{AA,0}$[a]	$[M]_0/[TTC]_0$[b]	$f_{AA,0}$[c]	Time (h)	Conv.[c] (mol%)			F_{AA}[c]	$DP_{n,th}$[d]	$M_{n,th}$[d] (kg mol^{-1})	SEC DMF	
						AA	CMAm	tot				M_n[e] (kg mol^{-1})	$Đ$[e]
*1***	H_2O	-	200	0	5	-	93	93	0	186	24.3	42.4	1.23
2	H_2O	0.02	195	0.07	24	100	100	100	0.07	195	24.8	45.7	1.29
3	H_2O	0.02	200	0.13	4.6	87	90	90	0.13	180	22.7	46.5	1.15
4	H_2O	0.02	200	0.20	6.7	73	76	75	0.19	150	19.3	37.3	1.10
5	0.03M HCl	0.00	200	0.14	4.5	92	93	93	0.13	192	24.1	37.5	1.26
6	0.03M HCl	0.00	200	0.20	4.6	89	87	87	0.20	174	21.7	28.1	1.29
7	0.03M HCl	0.00	200	0.30	7.2	84	85	85	0.30	170	20.6	36.7	1.10

[#] Polymerizations were performed in water at 45 °C in presence of $PDMAm_{36}$-TTC using VA-044 as a radical initiator (at an initial molar ratio of TTC/ VA-044: 1/0.2-0.35) at targeted solids contents of 10 wt%. [a] $\alpha_{AA,0}$ stands for the initial degree of ionization of AA monomer (i.e. in the polymerization medium at t = 0), which was calculated using $pK_{a,AA}$ = 4.26 by the Ostwald's dilution law (see the SI). [b] Initial molar ratio of ([CMAm] + [AA])/[$PDMAm_{36}$-TTC]. [c] Determined by ^{1}H NMR. [d] Theoretical number-average degree of polymerization, $DP_{n,th}$ and number-average molar mass, $M_{n,th}$, determined *via* the monomer conversion. [e] Number-average molar mass M_n, and dispersity, $Đ$, determined by SEC in DMF (+ LiBr 1g L^{-1}) with a PMMA calibration. **The synthesis and characterization of sample 1 has already been published before (see also the SI and Figure S2).[12]

In a first set of experiments, the molar fraction of AA in the feed ($f_{AA,0}$) was varied from 0 to 0.2 (*samples 1 to 4* in Table 1). The polymerizations were performed in deionized water, without the addition of acid or base. In these conditions, the degree of ionization (α) of AA monomer in the polymerization medium at t = 0 was calculated to be close to 2% in all cases ($\alpha_{AA,0}$ = 0.02 using pK_a (AA) = 4.26[43]). In a second series (*samples 5 to 7*), the polymerizations were performed in acidic aqueous medium (0.03M HCl), in order to completely protonate AA ($\alpha_{AA,0}$ = 0.00). Knowing that the presence of a single charge/chain can have a significant impact

on morphology and colloidal stability,[16,44] the goal was to investigate whether such a subtle change in $\alpha_{AA,0}$ towards full protonation of AA could have an impact on the polymerization and/or the nano-objects formed *in situ*. The experimental conditions and results are summarized in Table 1.

At the end of the polymerization after cooling to room temperature, most of the samples synthesized in deionized water or acidic water (*samples 1 to 7*) were slightly turbid indicating the formation of nano-objects. For the samples synthesized in deionized water (*samples 1 to 4*), increasing the AA content visually seemed to diminish the turbidity. *Samples 5 and 6* were viscous and turbid, while *sample 7*, synthesized at the highest AA content ($f_{AA,0}$ = 0.30), was only slightly turbid and less viscous (visually, similar to water). Based on the visual aspect of the samples, we concluded that the polymerizations should proceed through a dispersion polymerization mechanism.

In a previous work[28], we showed that the solution copolymerization of CMAm with AA in DMF was random. However, the solvent, pH and the polymerization process (homogenous *vs.* heterogeneous) can alter the apparent reactivity ratios in copolymerizations.[45–49] In order to study the incorporation of both comonomers in aqueous dispersion polymerization conditions, we monitored by ^{1}H NMR both series of dispersion copolymerizations, performed in pure water or in acidic water, respectively. As shown in Figure S3, in both conditions, CMAm and AA were consumed at a similar rate, leading to the formation of random copolymers without an obvious gradient, similar to the solution polymerization in DMF.[28] Considering the similar degree of ionization of AA in both cases, a similar reactivity is actually expected, and we can therefore conclude that the distribution of AA in the polymer chain is the same for both series of copolymerizations. In addition, the SEC analyses (Figure S4) revealed a good blocking efficiency independently of the molar fraction of AA in the feed and the presence (or absence)

of acid in the polymerization medium. The molar mass dispersities were below 1.3 (Table 1). A minor secondary population at the higher molar mass side was observed in particular for the runs with the highest monomer conversions. It was attributed to chain coupling, which is generally favored at high conversions. Compared to the homopolymerization of CMAm (*sample 1*), the copolymerization of CMAm with AA proceeded smoothly, and the SEC traces became more symmetric when the molar fraction of AA in the feed was increased: the *Đ* values decreased from about 1.3 to 1.1.

Cryo-TEM and small angle X-ray scattering (SAXS) performed at 1 wt% were used to determine the morphology of the nano-objects. Figure 1 shows the cryo-TEM images and SAXS profiles of the samples synthesized in deionized water, at natural pH. Regarding the cryo-TEM images, it is evident that the molar fraction of AA had an impact on the morphology: While the reference *sample 1* ($PDMAm_{36}$-*b*-$PCMAm_{186}$ synthesized without AA)[12] contained long nanoworms (Figure 1A and Figure S2A), *sample 2* with the lowest AA content ($f_{AA,0}$ = 0.07) contained much shorter worm-like objects. Interestingly, when $f_{AA,0}$ was increased to 0.13 and 0.2 (*samples 3 & 4*), the main morphology was spheres. Only on some areas on the cryo-TEM grids of *samples 3* and *4* the presence of nanometric worms was also observed.

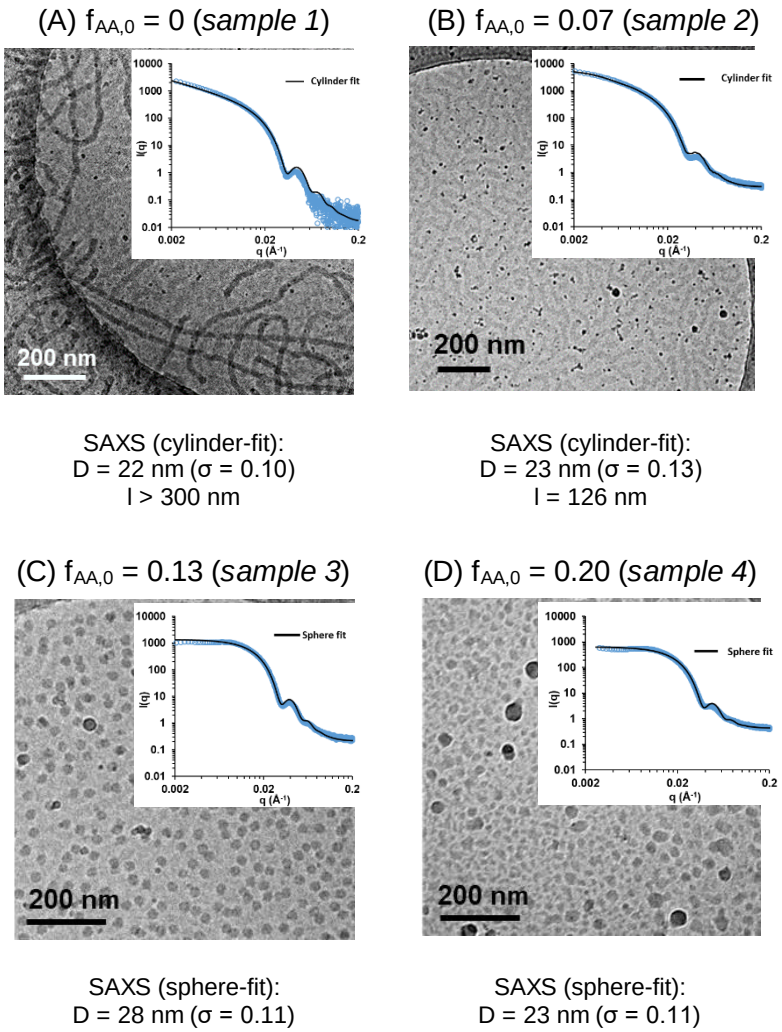

Figure 1. Representative cryo-TEM images and SAXS profiles at 25 °C (inserts) of $PDMAm_{36}$-*b*-P(CMAm-*co*-AA) samples synthesized at different $f_{AA,0}$ in deionized water. The samples were prepared at 1 wt% at room temperature in pure water. The dark spots are contaminations stemming from water crystals on the sample surface. D = diameter; l = length; σ = polydispersity of the diameter determined with a lognormal distribution.

The SAXS results displayed as inserts in Figure 1 clearly corroborated that the insertion of ≥ 13 mol% of AA units led to a change in morphology: spherical objects instead of cylindrical nano-assemblies were formed. As expected, the diameter of the spheres determined by SAXS (see Figure 1) was very close to the diameters of the fibers containing 7 mol% of AA (*D* = 23

nm, σ = 0.13) or 0 mol% of AA (*D* = 22 nm, σ = 0.10)[12] in the PCMAm block. It is worth noting that SAXS analyses confirmed a shorter fiber length for *sample* 2 containing 7 mol% of AA compared to reference *sample 1* without AA.

The second series of samples (*samples 5* to *7*) synthesized in acidic medium was also analyzed by the same techniques (Figure 2). Unlike the samples synthesized in deionized water, anisotropic worm-like nano-objects and no spherical particles were observed for quite large important fractions of AA in the second block (14 and 20% respectively, *samples 5* and *6*). Only for *sample 7*, with the highest amount of AA ($f_{AA,0}$ = 0.30), exclusively spherical nano-objects were formed instead of worm-like aggregates.

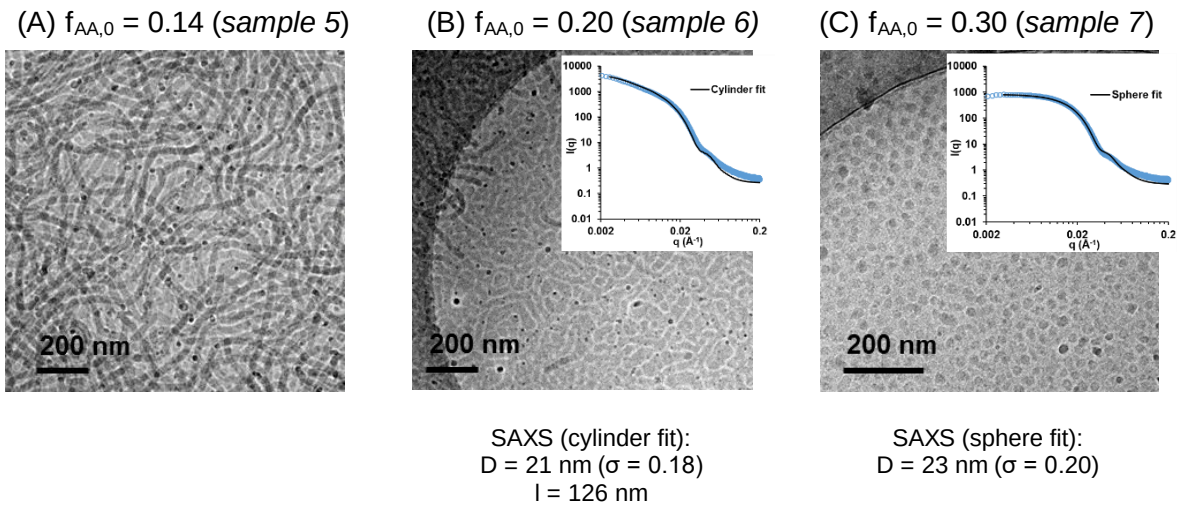

Figure 2. Representative cryo-TEM images and SAXS profiles at 25 °C (inserts) of $PDMAm_{36}$-*b*-P(CMAm-*co*-AA) samples synthesized at different $f_{AA,0}$ in acidic water. All samples were prepared at 1 wt% at room temperature in acidic water (0.03M HCl). D = diameter; l = length; σ = polydispersity of the diameter determined with a lognormal distribution.

Overall, the comparison of *samples 1 to 7* clearly demonstrates that the insertion of AA units into the PCMAm segment has a strong impact on the particle morphology formed during PISA, and that the impact is attenuated when AA is fully protonated. Given the random distribution of the comonomer in the hydrophobic block, we might explain this observation by

an overall change in the properties of the block, leading to a difference in the packing parameter.[27] In addition, the results clearly show that very small variations in the ionization degree of AA (α) (during synthesis) can actually have an impact on the morphologies formed. Comparing *sample 3* and *sample 5*, which contain similar molar fractions of AA, different morphologies are formed (spheres and worms respectively) although $\alpha_{AA,0}$ was only slightly decreased (from 0.02 to 0). Note that the worm morphology is the same for *sample 1*, *i.e.* a PDMAm-*b*-PCMAm diblock copolymer containing no AA units. As expected, the insertion of AA units into the PCMAm block has thus a greater impact on the morphology when the AA are partially deprotonated. In other words, a larger fraction of AA units (> 20 mol%) is required to trigger a change in morphology when the AA units are fully protonated.

To demonstrate the crucial importance of $\alpha_{AA,0}$ for the self-assembly occurring during polymerization, we synthesized an additional sample, with a monomer feed of $f_{AA,0} = 0.15$, and where AA was ionized to approximately 40 % by the addition of 0.4 equivalent of NaOH relative to AA (*sample 8*, Table S2). Again, the insertion of both comonomers was random (Figure S5A) and a good polymerization control was maintained (see SEC in Figure S5B and Table S2). In contrast to comparable samples synthesized in acidic conditions (*samples 3 and 5*), the sample was liquid and transparent. DLS analyses of *sample 8* at 0.1 and 1 wt% did not reveal the presence of nano-objects, as the scattering intensity was too low to determine of a reliable size. Therefore, we can conclude that in polymerization conditions where AA is ionized to about 40%, no self-assembly occurred, meaning that the polymerization occurred through a solution polymerization mechanism instead of PISA. The solubility of the diblock copolymer can reasonably be explained by the presence of charged monomer units that are randomly distributed in the P(CMAm-*co*-AA) block formed during polymerization.

In addition, we studied the influence of the degree of polymerization (*DP*) of the P(CMAm-*co*-AA) block, in order to evaluate whether it was possible to produce other morphologies than spheres and worms. In this series of experiments, we therefore varied the monomer/macroRAFT ratio, while keeping constant the monomer feed composition ($f_{AA,0}$ = 0.14), the ionization degree ($\alpha_{AA,0}$ = 0) and the targeted solids content (10 wt%) (see Table 2). Stable dispersions were formed in all cases and high monomer conversions were reached. The SEC analyses evidenced a good polymerization control and blocking efficiency (estimated close to 90%, Figure S6).

Table 2. Experimental conditions and results for aqueous copolymerizations of AA and CMAm in the presence of $PDMAm_{36}$ macroRAFT agent in acidic conditions.[#]

Entry	Solvent of polymerization	$[M]_0/[TTC]_0$[a]	$f_{AA,0}$[b]	Time (h)	Conv.[b] (mol%)			F_{AA}[b]	$DP_{n,th}$[c]	$M_{n,th}$[c] (kg mol^{-1})	SEC DMF	
					AA	CMAm	tot				M_n[d] (kg mol^{-1})	$Đ$[d]
9[a]	0.03M HCl	107	0.14	3.3	95	94	95	0.14	101	14.5	19.4	1.39
5[a]	0.03M HCl	207	0.14	4.5	92	93	93	0.13	192	24.1	37.5	1.26
10[a]	0.03M HCl	321	0.13	5.3	94	96	96	0.13	307	36.1	55.0	1.38

[#]Polymerizations were performed in water at 45 °C in presence of $PDMAm_{36}$-TTC, using VA-044 as a radical initiator (at an initial molar ratio of TTC/ VA-044 = 1/ 0.2 to 0.35) and an initial degree of ionization of AA, $\alpha_{AA,0}$ = 0, at targeted solids contents of 10 wt%. [a] Initial molar ratio of ([CMAm] + [AA])/[$PDMAm_{36}$-TTC]. [b] Determined by ^{1}H NMR. [c] Theoretical number-average degree of polymerization, $DP_{n,th}$ and number-average molar mass, $M_{n,th}$, determined *via* the monomer conversion. [d] Number-average molar mass M_n, and dispersity, $Đ$, determined by SEC in DMF (+ LiBr 1g L^{-1}) with a PMMA calibration.

Visually, *sample 9* with the shortest P(CMAm-*co*-AA) block was less turbid than *sample 5*, while *sample 10* with the longest P(CMAm-*co*-AA) block was a milky liquid. Cryo-

TEM analyses (Figure 3) revealed a clear impact of *DP* on morphology. Indeed, tiny spherical particles were observed for *sample 9* (DP_n ~ 100) - of which the size was confirmed by DLS measurements (D_z = 25 nm, PDI = 0.03) - while worms and well-defined vesicles were formed when the DP_n was increased to 192 (*sample 5*) and further to 307 (*sample 10*) respectively. This change in morphology with DP_n is similar to what was formerly described for PDMAm-*b*-PCMAm diblock copolymers (see reference[12] and Figure S2). We can thus conclude that the expected change in morphology with increasing DP_n from spheres to worms to vesicles is preserved when AA is incorporated into the PCMAm block. Interestingly, the cryo-TEM analyses showed no mixed morphologies but only pure morphologies, which is of particular interest in view of applications (in PISA mixed morphologies are often observed[50]).

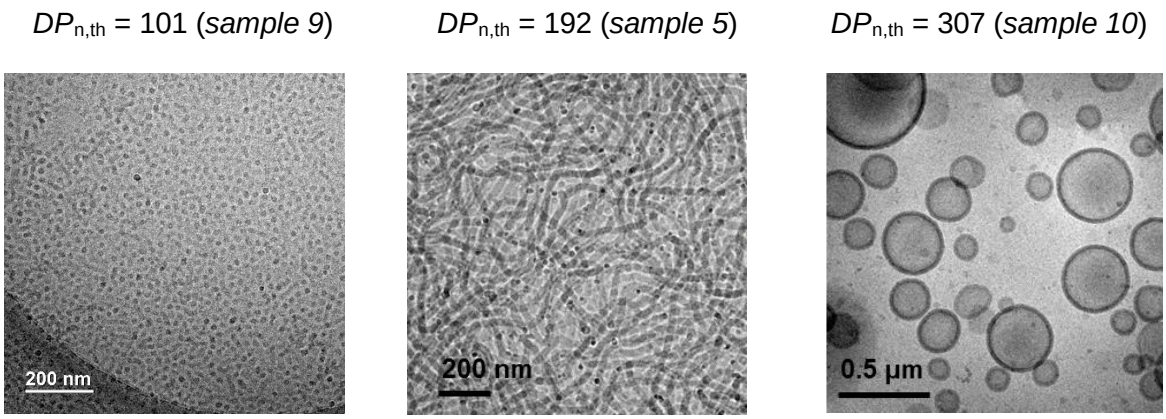

Figure 3. Representative cryo-TEM images of $PDMAm_{36}$-*b*-P(CMAm-*co*-AA) samples synthesized with three different hydrophobic lengths at constant $f_{AA,0}$ (~ 0.14) in acidic conditions. All samples were prepared at 1 wt% at room temperature in acidic water (0.03M HCl).

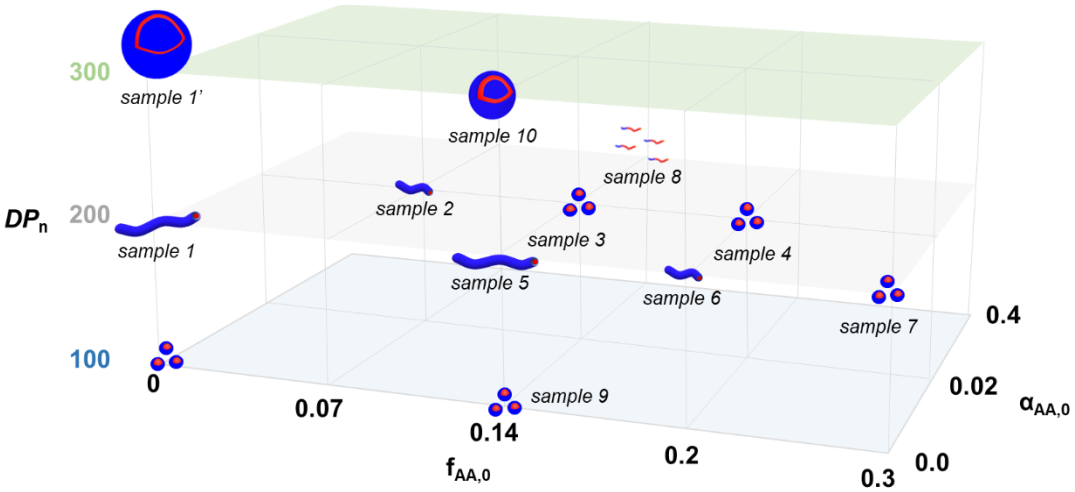

Figure 4. Attempt to rationalize the morphologies formed *via* PISA as a function of DP_n, initial molar fraction of AA ($f_{AA,0}$) and initial degree of ionization of AA in the polymerization medium ($\alpha_{AA,0}$).

As a summary, Figure 4 resumes the morphologies obtained as a function of the three variables studied: DP_n, the initial monomer composition ($f_{AA,0}$) and degree of ionization of AA in the feed ($\alpha_{AA,0}$). Overall, compared to simple PDMAm-*b*-PCMAm, the insertion of partially ionized AA has a much greater impact on morphology than fully protonated AA. In more detail, the results show that the insertion of small amounts of AA ($f_{AA,0} \leq 0.07$) into the PCMAm block does not change the polymerization mechanism nor the morphology, when the polymerization is performed in pure water. In contrast to acidic conditions, in pure water an AA molar fraction of around 14% is sufficient to induce a change in morphology (spheres instead of worms), while a considerable deprotonation of AA ($\alpha_{AA,0} \geq 0.4$) changes dramatically the polymerization process: no self-assembly occurs and soluble polymer chains are actually formed. In addition, increasing the molar percentage of AA in the polymerization medium to 30 mol% induced a change in morphology even when AA was fully protonated during polymerization: spheres instead of worm-like objects were formed.

3.2. Tuning morphology through addition of acid or base post-polymerization

Above, we have shown that not only the DP_n of the P(CMAm-*co*-AA) block, but also the initial degree of ionization of AA, $\alpha_{AA,0}$, in the polymerization medium, can have a crucial impact on the morphologies formed through PISA. In addition, when $\alpha_{AA,0}$ was high enough ($\alpha_{AA,0}$ ~ 0.4, *sample 8*), soluble PDMAm-*b*-P(CMAm-*co*-AA) diblock copolymer chains instead of block copolymer assemblies were formed.

Whereas we investigated in the previous section, the impact of the initial degree of ionization of AA ($\alpha_{AA,0}$) at which the PISA was performed, here we investigated the impact of modifying the degree of ionization of AA units after polymerization, α_{AA}, to answer the following questions: (i) Using soluble diblock copolymers synthesized in the presence of 0.4 equivalent base, is it possible to form the same morphologies as those formed by PISA, by adjusting α_{AA} post-polymerization through the addition of a strong acid? (ii) Can we trigger a change in morphology on nano-objects produced by PISA, by gradually adding a strong base after polymerization, while preventing complete disassembly into individual chains (unimers)? (iii) Is it possible to completely disassemble the PISA-formed nano-objects into individual chains by adding a sufficient quantity of base (and eventually reform the initial morphologies by successive addition of acid)?

To answer the first question, we took *sample 8* (soluble $PDMAm_{36}$-*b*-$P(CMAm_{0.85}$-*co*-$AA_{0.15})_{174}$ copolymer chains, the sample containing 0.4 equiv. of NaOH with respect to AA units) and progressively decreased α_{AA} from 0.4 to 0.0 by gradually adding small volumes of 1M HCl to trigger chain assembly post-polymerization.

While at α_{AA} ~ 0.4 no nano-objects were detected by DLS measurements, at α_{AA} = 0.2 (addition of 0.5 equiv. of HCl with respect to NaOH) tiny aggregates (D_z = 34 nm) were

measured by DLS, of which the size slightly increased when α_{AA} was further decreased (Figure S7A). At α_{AA} = 0, the z-average diameter increased significantly and the size distribution broadened. Cryo-TEM analysis of the sample at α_{AA} = 0 revealed a mixture of spheres and worms, with the latter being the predominant species (Figure S7B). The morphologies formed are significantly different from *sample 5* (comparable composition but synthesized by PISA at $\alpha_{AA,0}$ = 0) for which exclusively long nanofibers were produced (Figure 2A). We can thus conclude that the self-assembly of the polymer chains can be induced post-polymerization by the addition of acid. However, the assemblies are different from those formed during PISA, even though they were produced at the same α_{AA}. It should be noted, that the decrease in α was performed by progressively adding a strong acid to the sample at 1 wt%, whereas the worms were formed at 10 wt% during PISA. Different hypotheses can thus be proposed to explain the difference in the morphologies obtained: We can postulate (1) an impact of the polymer concentration on the self-assembly or (2) kinetic effects, assuming that the final morphologies are not at thermodynamic equilibrium.

To answer the second (ii) and the third (iii) question concerning pH-induced morphological transitions, we progressively added small amounts of a strong base (NaOH) to the vesicles produced at $\alpha_{AA,0}$ = 0 (*sample 10*, PDMAm$_{36}$-*b*-P(CMAm$_{0.87}$-*co*-AA$_{0.13}$)$_{307}$). Acrylic acid (AA) being a weak acid, the degree of ionization of the AA units in the polymer chains can again be directly calculated knowing the molar ratio of NaOH/AA units. Interestingly, a slight increase in α_{AA} from 0 to 0.06 (through the addition of 0.06 equiv. of NaOH relative to AA[†]) induced a clear morphological transition from vesicles to worms (Figures 5A and 5B). Further increasing α_{AA} to 0.16 resulted in a mixture of spheres and fibers (Figure 5C), and at α_{AA} = 0.38 only tiny

[†] taking into account the number of moles of HCl initially present in the polymerization medium

spherical nano-objects (Figure 5D) were obtained. When α_{AA} was finally increased to 0.77 (addition of 0.77 equiv. of NaOH relative to AA†), a very low scattering intensity and diameters compatible with unimers were measured by DLS (Figure S8), which indicates the dissociation of the aggregates into soluble chains. Comparing *sample 10* and *8*, the critical value of α_{AA}, at which disassembly occurs, depends on the DP_n of the solvophobic block. Furthermore, we confirmed with *sample 6* ($PDMAm_{36}$-*b*-$P(CMAm_{0.80}$-*co*-$AA_{0.20})_{174}$, synthesized at $\alpha_{AA,0} = 0$) that it is also possible to dissociate PISA-produced worms into individual chains. Increasing α_{AA} to 0.45 (by adding 0.45 equiv. of 1M NaOH†) led to an abrupt decrease in turbidity. The DLS measurements showed a scattering intensity close to water and diameters which are consistent with the formation of unimers (Figure S9), suggesting again the complete dissolution of the polymer chains.

The reversibility of the base- and acid-induced dissociation/assembly process was also assessed. After complete dissolution of the vesicles (*sample 10*, after adjustment of α_{AA} to 0.77), the solution was again acidified to $\alpha_{AA} = 0.0$ using HCl, following two distinct protocols. In the first experiment, HCl was added in one shot to the sample at 1 wt%. Compared to the initial vesicles for which a z-average diameter D_z of 292 nm (PDI = 0.49) was determined, a lower dispersity (PDI = 0.09) and a significantly smaller diameter (D_z = 75 nm) were evidenced by DLS. In addition, cryo-TEM analysis of the sample clearly showed the production of tiny vesicles with a small void, in addition to flat lamellar objects[51] (Figure 5E). The addition of acid thus triggered the assembly of the chains into nanometric objects as expected, however, the dimensions are completely different. These differences might again be explained by concentration effects (the reassembly was triggered at 1 wt% whereas PISA was performed at about 10 wt%) or by the formation of out-of-the equilibrium structures at $\alpha_{AA} = 0$. We have therefore performed an additional experiment, where we added the acid to a concentrated solution (8 wt%) of the dissolved diblock copolymer. Again, a variety of objects was formed,

similar to the ones obtained in the former experiment, where the acid was added to a solution at 1 wt%. We can thus conclude that the assemblies are certainly not at their thermodynamic equilibrium, but that their formation was kinetically controlled.

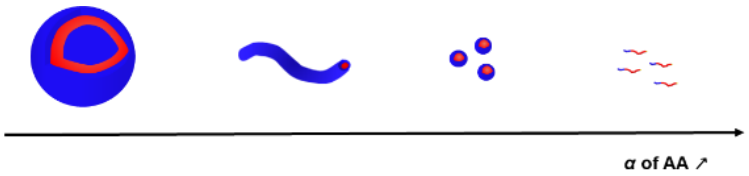

A Pristine (α_{AA} = 0.00 at 1 wt%)

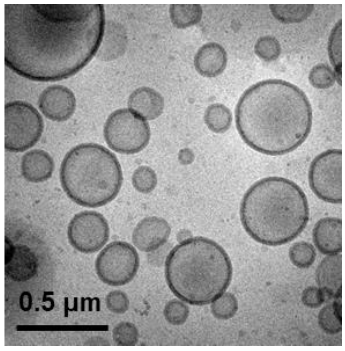

B Increase to α_{AA} = 0.06 post-polym. (at 1 wt%)

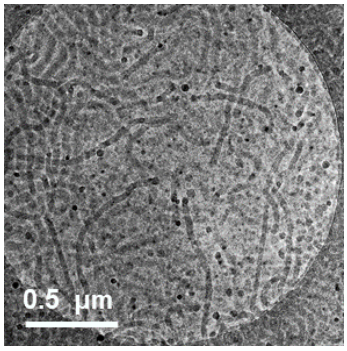

C Increase to α_{AA} = 0.16 post-polym. (at 1 wt%)

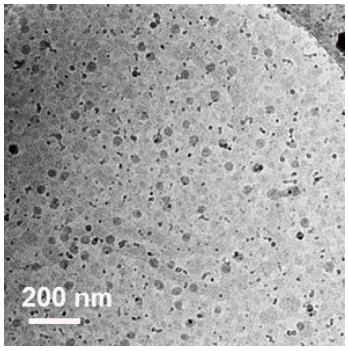

D Increase to α_{AA} = 0.38 (at 1 wt%)

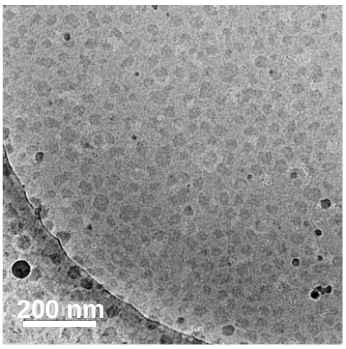

E Decrease to α_{AA} = 0.00 at 1 wt% (after complete dissociation at α_{AA} = 0.77)

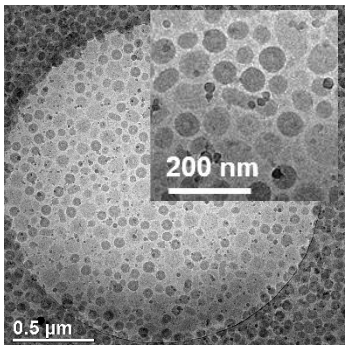

F Decrease to α_{AA} = 0.00 at 8 wt% (after complete dissociation at α_{AA} = 0.77)

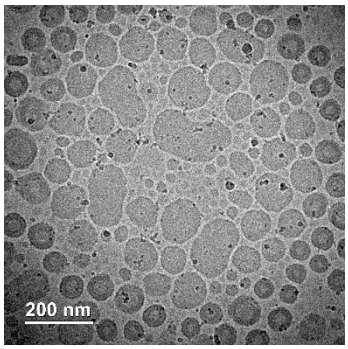

Figure 5. Representative cryo-TEM images of (A) the pristine aqueous dispersion of PDMAm$_{36}$-*b*-P(PCMAm$_{0.87}$-*co*-AA$_{0.13}$)$_{307}$ (*sample 10*) prepared at 1 wt%, at room temperature and analyzed at α_{AA} = 0. Sample after progressive addition of 1M NaOH post-polymerization to (B) α_{AA} = 0.06, (C) α_{AA} = 0.16 and (D) α_{AA} = 0.38. After disassembly by addition of NaOH post-

polymerization to $\alpha_{AA} = 0.77$, the sample was set again to $\alpha_{AA} = 0$ through additional of HCl, (E) at 1 wt% and (F) at 8 wt%.

In conclusion, we have seen that the modification of the degree of ionization after polymerization enabled the formation of nano-objects from initially dissolved PDMAm-*b*-P(CMAm-*co*-AA) diblock copolymers chains. However, a mixture of morphologies was formed that were less well-defined than the nano-objects obtained by PISA in comparable conditions. This result is crucial and highlights the interest of the PISA process because it shows that the objects obtained as pure morphologies *via* a simple PISA process, cannot be formed straightforwardly post-polymerization. Reversely, assemblies that were formed at a low degree of ionization ($\alpha_{AA,0} \leq 0.02$) could be disassembled into unimers by the addition of base. The disassembly of the preformed nano-objects occurred at $\alpha_{AA} > 0.4$, which was similar to the conditions that formerly hampered the self-assembly of the polymer chains during polymerization. Finally, most interestingly, we showed that a given diblock copolymer assembly can transform, post-polymerization, from vesicles, to worms, to spheres by the simple addition of a strong base (though the progressive deprotonation of the weakly acidic AA units).

3.3. Temperature-responsiveness

As mentioned above, we have previously shown that PCMAm homopolymers may exhibit an UCST-type transition in aqueous solution.[28] Based on studies of the structurally similar P(Am-*co*-AN) statistical copolymers, their thermo-responsiveness was attributed to the combination of both amide and carbonitrile functional groups within the polymer chain, where amide groups can interact through inter- and intramolecular H-bonds, whereas carbonitriles interact through dipole-dipole interactions.[28,52] However, the UCST behavior of PCMAm was

only observed for sufficiently low molar masses (roughly below 10 kg mol^{-1}, *i.e.* below DP_n ~ 100),[28] which are actually lower than the molar masses of most of the samples studied here. Longer PCMAm polymer chains were insoluble in water. In addition, we had shown that random insertion of acrylic acid units - yielding random P(CMAm-*co*-AA) copolymers - considerably decreased the clearing point (T_{CP}) to lower temperatures. For instance, the T_{CP} of a copolymer containing 13 mol% of AA (F_{AA}= 0.13), P($CMAm_{0.87}$-*co*-$AA_{0.13}$)$_{50}$, was reduced by more than 20 °C compared to the PCMAm homopolymer.[28] We had also shown that the pH had a great influence on the thermo-responsive behavior of P(CMAm-*co*-AA) copolymers: the T_{CP} decreased when the pH, and hence α_{AA}, was increased. In a related study, we showed that PDMAm-*b*-PCMAm diblock copolymer assemblies prepared by PISA in water exhibit a complex response to temperature.[12] Therefore, we can reasonably expect that the PDMAm-*b*-P(CMAm-*co*-AA) assemblies prepared by PISA are thermoresponsive, and we therefore studied systematically their temperature-responsiveness by turbidimetry.

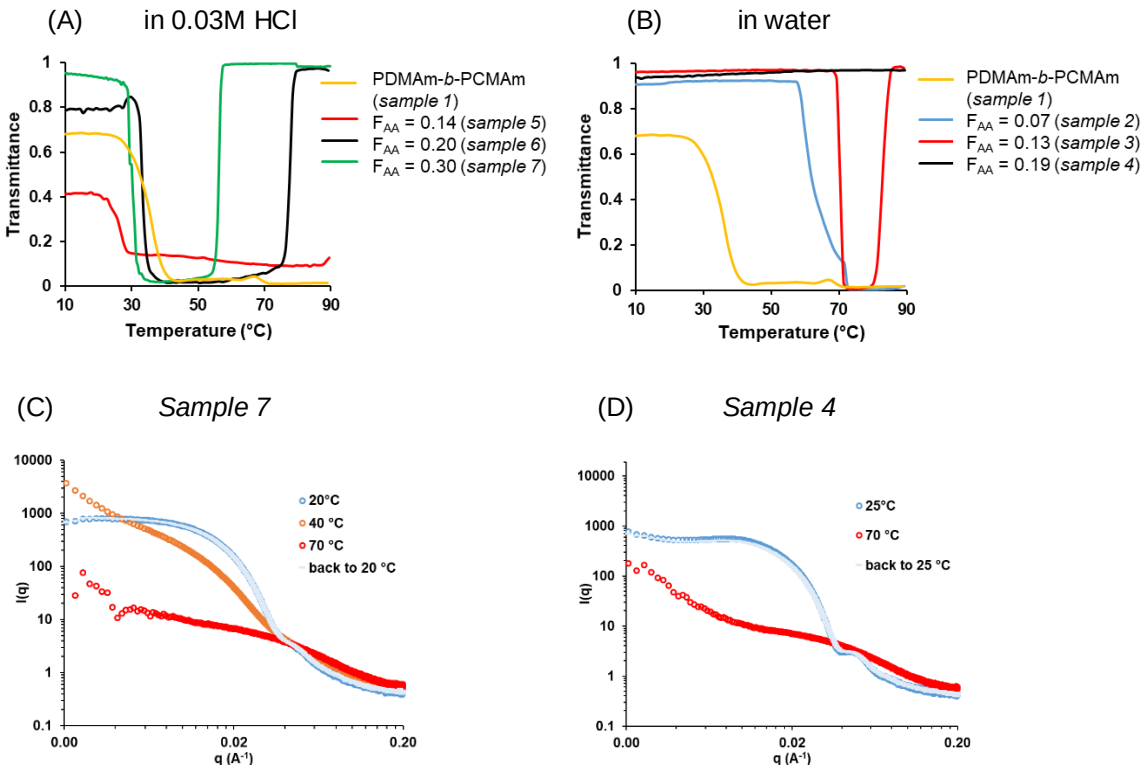

Figure 6. Turbidity curves of PDMAm-*b*-P(CMAm-*co*-AA) with different F_{AA} synthesized and analyzed (A) in acidic water ([HCl] = 0.03M) and (B) deionized water, prepared at 1 wt% (cooling step, λ = 670 nm, 1 °C min^{-1}). Evolution of SAXS profiles with temperature for (C) sample 7 and (D) sample 4 (analysed at 1 wt%).

For *samples 5*, *6* and *7*, synthesized and analyzed in acidic water, we observed a strong influence of the AA content on the temperature-responsive behavior by turbidimetry measurements (Figure 6A). For the reference *sample 1*, comprising no AA, a LCST-like transition with a cloud point around 35 °C was observed, while *sample 5* with the F_{AA} = 0.14 had a low transmittance value at all temperatures and presented a decrease in transmittance at about 25 °C. It should be reminded that these samples contained worm-like assemblies. Based on our previous studies,[12] we can reasonably assume that the loss of transmittance can be

attributed to a secondary aggregation of the assemblies. Indeed, DLS analyses of *sample 5* at different temperatures showed the formation of larger aggregates upon temperature increase, which supports this hypothesis (Figure S10A).

Interestingly, for *samples 6* and *7* containing higher contents of AA (F_{AA} = 0.20 and 0.30) both a LCST and an UCST-like transitions were observed. In our previous study, we observed a similar behavior for a low molar mass diblock copolymer, $PDMAm_{23}$-*b*-$PCMAm_{93}$. We assumed that the clouding of the solution was again caused by an aggregation mechanism; however, the subsequent clearing could be caused either by the reversibility of the secondary aggregation yielding individual nano-objects or by the complete dissociation of the aggregates into individual chains. Considering that the transmission at high temperatures (above the clearing point) is even higher than the initial one (below the cloud point), the second explanation is more likely. To better understand the apparent LCST-UCST transition, *sample 7* (F_{AA} = 0.30, $\alpha_{AA,0}$ = 0.00) containing spherical nano-objects, was also investigated by temperature-dependent SAXS analyses at 1 wt%, displayed in Figure 6C. The data are consistent with the formation of large, ill-defined objects at 40 °C, presumably through an aggregation and reorganization process of the original spherical particles. The suggested associative phenomenon is supported by the obvious increase in scattering intensity at low q values in SAXS and the disappearance of any correlation peaks. Upon further heating to 70 °C, the scattering intensity at low q values drops significantly, whereas it increases slightly at higher q values. Furthermore, instead of a plateau, the scattering intensity increases towards low q values. Such profile is typically observed for individual Gaussian chains that are weakly interacting.[8] Overall, we can thus conclude that upon a progressive increase in temperature, the small nanospheres first aggregate and reorganize, which is evidenced by a decrease of the transmittance in turbidimetry (Figure 6A) and visible as a cloud point. Upon further temperature increase, the solution clears up. The clearing point corresponds to the temperature at which the

aggregates dissolve molecularly into individual chains.[8] Importantly, as evidenced by SAXS, the transition was fully reversible since identical signals were obtained when the sample was cooled back to room temperature. The results are thus consistent with the suggested reversible temperature-dependent aggregation mechanism. A similar combined LCST-UCST-type behavior has been reported in the literature for neutral PEG-*b*-P(AN-*co*-Am) diblock copolymers, which exhibited a similar clouding and then clearing behavior upon heating, which was solely explained by a reversible secondary aggregation of the nano-objects.[53] Regarding the turbidimetry plot, a similar mechanism (aggregation followed by dissolution – though shifted in temperature) can be assumed for *sample 6* (F_{AA} = 0.20) containing worm-like instead of spherical nano-objects. DLS analyses performed at various temperatures (Figure S10B) confirmed this assumption. While larger aggregates were initially formed upon heating, further heating led to their disassembly into individual chains.

Figure 6B displays the turbidity measurements for *samples 2*, *3* and *4*, which were all synthesized and analyzed in water (without adjusting α_{AA}). Again, we observed a strong influence of the AA content on the temperature-responsive behavior. However, despite the small change in α_{AA}, their behavior was significantly different from *samples 5 to 7* displayed in Figure 6A, which were fully protonated. For the sample containing the highest amount of AA (F_{AA} = 0.19, *sample 4*), independently of the temperature, the transmittance was close to 1. It is actually interesting to compare this *sample 4* to the formerly discussed *sample 7* (Figure 5C) because they both contain tiny spherical particles with a diameter about 20 nm. Even though no significant evolution was observed for *sample 4* by turbidimetry, the SAXS analyses (at 1 wt%) displayed in Figure 6D revealed a clear drop in the scattering intensity upon heating to 70 °C. The scattering profile is indeed similar to *sample 7* at 70 °C and consistent with weakly interacting block copolymers chains, suggesting that the spherical assemblies dissolved into unimers upon heating. Again, the transition was fully reversible, as shown by the overlay of the

signals at 25 °C before and after a heating cycle. In contrast, turbidimetry of *sample 3* (F_{AA} = 0.13) revealed a complex transition with a LCST-type transition around 70 °C (confirmed by SAXS, see Figure S11B), followed by a UCST transition above 80 °C. This behavior is similar to *samples 6 and 7*, although the temperature range for which aggregation occurs is much smaller. For *sample 2*, which contains the smallest amount of AA units (F_{AA} = 0.07), we observed only a LCST-type transition above 60 °C, which was again attributed to an aggregation mechanism characterized by an increased scattering intensity at low q values (Figure S11A). Compared to PDMAm-*b*-PCMAm diblock copolymer[12], overall, the presence of some deprotonated acrylic acid units in the hydrophobic block improves the colloidal stability to temperature increase, because the cloud points is shifted to higher temperatures. In addition, the presence of sufficient AA units can even lead to the molecular dissolution of the polymers at sufficiently high temperatures. Compared to the fully protonated samples, the impact of AA on assembly and thermo-responsiveness is greater when the AA units are (partially) ionized. It might be added, that *sample 8* (soluble diblock copolymers chains, synthesized and studied at α_{AA} = 0.41) did not show any thermal transition over the temperature range (10 to 90 °C) studied by turbidimetry. As expected, the presence of charged AA units is responsible for the formation of fully hydrophilic diblock polymer chains, which are not sensitive to temperature.

In the above study, the samples were analyzed in the same solvent as the one used for the synthesis of the nano-objects (water or diluted HCl solution). In principle, it should be possible to tune the thermo-responsiveness by changing the ionization degree, at which the samples are analyzed. From our previous study, we know that the addition of an acid or base also changes the chain assembly, and this must be taken into account when investigating the influence of the ionization degree α_{AA} on thermo-responsiveness. We selected *sample 6* and *sample 8* as representative samples and investigated the impact of modifying α post-polymerization. In

order to increase or decrease α_{AA}, we used a 0.10 M NaOH solution for *sample 6* (synthesized at α_{AA} = 0.0, worms) and a 0.12 M HCl solution for *sample 8* (synthesized at α_{AA} = 0.41, soluble). When *sample 6* was analyzed at α_{AA} = 0.45 (through the addition of 0.45 equiv. of NaOH relative to AA†) by turbidimetry, in contrast to the analysis in acidic medium (α_{AA} = 0) (Figure 6), we did not observe any thermal transition (Figure S12A). The negative charges on the AA units certainly induced the complete dissociation of the nano-object (as discussed previously), explaining the high transmittance observed over the complete temperature range (10 to 90 °C). For *sample 8*, we know that the decrease of α_{AA} towards lower values - leading to the complete protonation of the AA units – resulted in the formation of nano-objects (Figure S7). At α_{AA} = 0, this sample clearly exhibited the above-observed LCST- and UCST-type thermal transitions (Figure S12B), which can reasonably be explained by a temperature triggered-secondary aggregation followed by a dissolution of the chains, as described for *sample 6* (see Figure S10B).

In view of these results, we can conclude that the molar fraction of AA in the PCMAm block has a great impact on the thermoresponsive behavior of the dispersions and that this behavior strongly depends on the AA units' ionization degree. In general, a higher fraction of AA favors the colloidal stability of the nano-objects upon temperature increase. Comparing dispersions in acidic medium and in water, the dispersions were more stable in water, where a smaller window of LCST/UCST-like transition or no LCST transition was observed, even though the difference in protonation must be very low.

4. Discussion and conclusions

In conclusion, we report for the first time the combination of two functional monomers promoting the formation of pH- and thermo-responsive core blocks in a typical aqueous RAFT-

mediated PISA. PDMAm was selected as a neutral stabilizing block, while the assembling block was composed of PCMAm containing AA units. A series of polymerizations were performed by varying three parameters, namely the molar fraction of AA in the polymerization feed ($f_{AA,0}$), the degree of ionization of AA ($\alpha_{AA,0}$), and the degree of polymerization (DP_n) of the solvophobic block. In all cases, a good blocking efficiency was observed with a random incorporation of the AA units into the PCMAm block. All main morphologies of PISA, namely nanospheres, worms or vesicles, could be formed as pure phases through the variation of the three parameters. While it was expected that the molar mass would have an impact on morphology, the strong influence of the incorporation of AA and in particular its degree of ionization on morphology was less expected. By varying either of the parameters, we have shown that it was possible, for instance, to produce selectively worms or spherical nanoparticles, while keeping constant the molar mass of the polymer blocks. This means that one single copolymer composition can yield different morphologies through the same process. In particular conditions, when α was high enough, soluble diblock copolymers chains were formed, meaning that the polymerization proceeded through a solution polymerization mechanism.

Furthermore, we have demonstrated that the nanoassemblies exhibit an unprecedented, complex responsiveness to changes in temperature and to the addition of acid/base. The latter can efficiently trigger morphological transitions, through the controlled deprotonation or protonation of the AA units in the solvophobic core. For instance, vesicles can transform into worms, spheres or soluble chains, but these morphological transitions are only partially reversible. As such, the original vesicles obtained through PISA were much more homogeneous in shape and size than those formed after a complete base-acid addition cycle, highlighting the interest of the PISA process for the production of uniform morphologies. While the addition of acid or base is a way to induce morphological transitions or disassembly, temperature

modification can also be used to trigger phase transitions. Distinct formulations possess both a cloud and a clearing point, which were explained by secondary aggregation of primary aggregates and chain dissolution, respectively. We highlighted that high F_{AA} contents tends to expand the window of colloidal stability, *i.e.* diminishes the temperature range where secondary aggregates exist. Similarly, a very slight increase in α_{AA} (induced by the change of solvent used from acidic 0.03M HCl to deionized water) improves the colloidal stability due to the presence of anionic charges on the AA units providing more stability. Consequently, when F_{AA} and α_{AA} are sufficiently high, no cloud point is observed. For instance, for copolymers with $F_{AA} \geq 0.2$ in water, no LCST-like behavior, but only the dissolution of the assemblies at high temperature, typical of UCST diblock copolymers, is observed. We believe that this complex responsiveness is due to the design of diblock copolymers incorporating both pH- and thermoresponsive units in the solvophobic block, which has never been reported in PISA before. The ease and scalability of the synthesis process in addition to the tunability of the response should pave the way towards many applications.

Supporting Information. Detailed methods and additional results [Synthesis of the PDMAm macroRAFT agent; Calculation of the degree of ionization of AA; Recently published results for PDMAm-*b*-PCMAm diblock copolymers for comparison; Additional characterizations of the PDMAm-*b*-P(CMAm-*co*-AA) copolymers; Modification of α_{AA} post-polymerization; Additional characterization of the thermo-responsive properties of samples PDMAm-*b*-P(CMAm-*co*-AA)]

Acknowledgements. We thank SOLEIL for the provision of synchrotron radiation facilities. We are grateful to Dr. Thomas Bizien for his help to use the “swing” beamline (proposal number 20201382 and 20220204) and to the SOLEIL staff for smoothly running the facility. This work benefited from the use of the SasView application, originally developed

under NSF award DMR-0520547. SasView contains code developed with funding from the European Union's Horizon 2020 research and innovation program under the SINE2020 project, grant agreement No 654000. We thank Clement Debrie (IPCM) for data SAXS treatments and Rayane Hamdoun for the technical support.

References

(1) Wan, W.-M.; Sun, X.-L.; Pan, C.-Y. Morphology Transition in RAFT Polymerization for Formation of Vesicular Morphologies in One Pot. *Macromolecules* **2009**, *42* (14), 4950–4952. https://doi.org/10.1021/ma901014m.

(2) Li, Y.; Armes, S. P. RAFT Synthesis of Sterically Stabilized Methacrylic Nanolatexes and Vesicles by Aqueous Dispersion Polymerization. *Angewandte Chemie International Edition* **2010**, *49* (24), 4042–4046. https://doi.org/10.1002/anie.201001461.

(3) Boissé, S.; Rieger, J.; Belal, K.; Di-Cicco, A.; Beaunier, P.; Li, M.-H.; Charleux, B. Amphiphilic Block Copolymer Nano-Fibers via RAFT-Mediated Polymerization in Aqueous Dispersed System. *Chemical Communications* **2010**, *46* (11), 1950. https://doi.org/10.1039/b923667h.

(4) Rieger, J. Guidelines for the Synthesis of Block Copolymer Particles of Various Morphologies by RAFT Dispersion Polymerization. *Macromolecular Rapid Communications* **2015**, *36* (16), 1458–1471. https://doi.org/10.1002/marc.201500028.

(5) D'Agosto, F.; Rieger, J.; Lansalot, M. RAFT-Mediated Polymerization-Induced Self-Assembly. *Angewandte Chemie International Edition* **2020**, *59* (22), 8368–8392. https://doi.org/10.1002/anie.201911758.

(6) Pei, Y.; Lowe, A. B.; Roth, P. J. Stimulus-Responsive Nanoparticles and Associated (Reversible) Polymorphism via Polymerization Induced Self-Assembly (PISA). *Macromolecular Rapid Communications* **2017**, *38* (1), 1600528. https://doi.org/10.1002/marc.201600528.

(7) Le, D.; Keller, D.; Delaittre, G. Reactive and Functional Nanoobjects by Polymerization-Induced Self-Assembly. *Macromolecular Rapid Communications* **2019**, *40* (2), 1800551. https://doi.org/10.1002/marc.201800551.

(8) Cunningham, V. J.; Ratcliffe, L. P. D.; Blanazs, A.; Warren, N. J.; Smith, A. J.; Mykhaylyk, O. O.; Armes, S. P. Tuning the Critical Gelation Temperature of Thermo-Responsive Diblock Copolymer Worm Gels. *Polym. Chem.* **2014**, *5* (21), 6307–6317. https://doi.org/10.1039/C4PY00856A.

(9) Ratcliffe, L. P. D.; Derry, M. J.; Ianiro, A.; Tuinier, R.; Armes, S. P. A Single Thermoresponsive Diblock Copolymer Can Form Spheres, Worms or Vesicles in

Aqueous Solution. *Angewandte Chemie International Edition* **2019**, *58* (52), 18964–18970. https://doi.org/10.1002/anie.201909124.

(10) Le, D.; Wagner, F.; Takamiya, M.; Hsiao, I.-L.; Gil Alvaradejo, G.; Strähle, U.; Weiss, C.; Delaittre, G. Straightforward Access to Biocompatible Poly(2-Oxazoline)-Coated Nanomaterials by Polymerization-Induced Self-Assembly. *Chemical Communications* **2019**, *55* (26), 3741–3744. https://doi.org/10.1039/C9CC00407F.

(11) Byard, S. J.; O'Brien, C. T.; Derry, M. J.; Williams, M.; Mykhaylyk, O. O.; Blanazs, A.; Armes, S. P. Unique Aqueous Self-Assembly Behavior of a Thermoresponsive Diblock Copolymer. *Chem. Sci.* **2020**, *11* (2), 396–402. https://doi.org/10.1039/C9SC04197D.

(12) Audureau, N.; Coumes, F.; Veith, C.; Guibert, C.; Guigner, J.-M.; Stoffelbach, F.; Rieger, J. Synthesis and Characterization of Temperature-Responsive N-Cyanomethylacrylamide-Containing Diblock Copolymer Assemblies in Water. *Polymers* **2021**, *13* (24), 4424. https://doi.org/10.3390/polym13244424.

(13) Deane, O. J.; Jennings, J.; Armes, S. P. Shape-Shifting Thermoreversible Diblock Copolymer Nano-Objects *via* RAFT Aqueous Dispersion Polymerization of 4-Hydroxybutyl Acrylate. *Chem. Sci.* **2021**, *12* (41), 13719–13729. https://doi.org/10.1039/D1SC05022B.

(14) Cumming, J. M.; Deane, O. J.; Armes, S. P. Reversible Addition-Fragmentation Chain Transfer Aqueous Dispersion Polymerization of 4-Hydroxybutyl Acrylate Produces Highly Thermoresponsive Diblock Copolymer Nano-Objects. *Macromolecules* **2022**, *55* (3), 788–798. https://doi.org/10.1021/acs.macromol.1c02431.

(15) Audureau, N.; Coumes, F.; Guigner, J.-M.; Nguyen, T. P. T.; Ménager, C.; Stoffelbach, F.; Rieger, J. Thermoresponsive Properties of Poly(Acrylamide- *Co* -Acrylonitrile)-Based Diblock Copolymers Synthesized (by PISA) in Water. *Polym. Chem.* **2020**, *11* (37), 5998–6008. https://doi.org/10.1039/D0PY00895H.

(16) Lovett, J. R.; Warren, N. J.; Ratcliffe, L. P. D.; Kocik, M. K.; Armes, S. P. PH-Responsive Non-Ionic Diblock Copolymers: Ionization of Carboxylic Acid End-Groups Induces an Order-Order Morphological Transition. *Angew. Chem. Int. Ed.* **2015**, *54* (4), 1279–1283. https://doi.org/10.1002/anie.201409799.

(17) Deng, R.; Derry, M. J.; Mable, C. J.; Ning, Y.; Armes, S. P. Using Dynamic Covalent Chemistry To Drive Morphological Transitions: Controlled Release of Encapsulated Nanoparticles from Block Copolymer Vesicles. *Journal of the American Chemical Society* **2017**, *139* (22), 7616–7623. https://doi.org/10.1021/jacs.7b02642.

(18) Ratcliffe, L. P. D.; Couchon, C.; Armes, S. P.; Paulusse, J. M. J. Inducing an Order–Order Morphological Transition via Chemical Degradation of Amphiphilic Diblock Copolymer Nano-Objects. *Biomacromolecules* **2016**, *17* (6), 2277–2283. https://doi.org/10.1021/acs.biomac.6b00540.

(19) Baddam, V.; Välinen, L.; Kuckling, L.; Tenhu, H. Morphological Transitions of Cationic PISA Particles by Salt, Triflate Ions and Temperature; Comparison of Three Polycations. *Polym. Chem.* **2022**, *13* (25), 3790–3799. https://doi.org/10.1039/D2PY00301E.

(20) Mellot, G.; Beaunier, P.; Guigner, J.-M.; Bouteiller, L.; Rieger, J.; Stoffelbach, F. Beyond Simple AB Diblock Copolymers: Application of Bifunctional and Trifunctional RAFT Agents to PISA in Water. *Macromolecular Rapid Communications* **2019**, *40* (2), 1800315. https://doi.org/10.1002/marc.201800315.

(21) Zhang, Q.; Zeng, R.; Zhang, Y.; Chen, Y.; Zhang, L.; Tan, J. Two Polymersome Evolution Pathways in One Polymerization-Induced Self-Assembly (PISA) System. *Macromolecules* **2020**, *53* (20), 8982–8991. https://doi.org/10.1021/acs.macromol.0c01624.

(22) Ikkene, D.; Arteni, A. A.; Ouldali, M.; Six, J.-L.; Ferji, K. Self-Assembly of Amphiphilic Copolymers Containing Polysaccharide: PISA versus Nanoprecipitation, and the Temperature Effect. *Polym. Chem.* **2020**, *11* (29), 4729–4740. https://doi.org/10.1039/D0PY00407C.

(23) Zhou, D.; Dong, S.; Kuchel, R. P.; Perrier, S.; Zetterlund, P. B. Polymerization Induced Self-Assembly: Tuning of Morphology Using Ionic Strength and PH. *Polymer Chemistry* **2017**, *8* (20), 3082–3089. https://doi.org/10.1039/C7PY00552K.

(24) Hunter, S. J.; Penfold, N. J. W.; Chan, D. H.; Mykhaylyk, O. O.; Armes, S. P. How Do Charged End-Groups on the Steric Stabilizer Block Influence the Formation and Long-Term Stability of Pickering Nanoemulsions Prepared Using Sterically Stabilized Diblock Copolymer Nanoparticles? *Langmuir* **2020**, *36* (3), 769–780. https://doi.org/10.1021/acs.langmuir.9b03389.

(25) Penfold, N. J. W.; Lovett, J. R.; Warren, N. J.; Verstraete, P.; Smets, J.; Armes, S. P. PH-Responsive Non-Ionic Diblock Copolymers: Protonation of a Morpholine End-Group Induces an Order–Order Transition. *Polymer Chemistry* **2016**, *7* (1), 79–88. https://doi.org/10.1039/C5PY01510C.

(26) Xu, X.-F.; Pan, C.-Y.; Zhang, W.-J.; Hong, C.-Y. Polymerization-Induced Self-Assembly Generating Vesicles with Adjustable PH-Responsive Release Performance. *Macromolecules* **2019**, No. 52, 1965–1975.

(27) Zhang, J.; Farias-Mancilla, B.; Kulai, I.; Hoeppener, S.; Lonetti, B.; Prévost, S.; Ulbrich, J.; Destarac, M.; Colombani, O.; Schubert, U. S.; Guerrero-Sanchez, C.; Harrisson, S. Effect of Hydrophilic Monomer Distribution on Self-Assembly of a PH-Responsive Copolymer: Spheres, Worms and Vesicles from a Single Copolymer Composition. *Angewandte Chemie International Edition* **2021**, *60* (9), 4925–4930. https://doi.org/10.1002/anie.202010501.

(28) Audureau, N.; Veith, C.; Coumes, F.; Nguyen, T. P. T.; Rieger, J.; Stoffelbach, F. RAFT-Polymerized N-Cyanomethylacrylamide-Based (Co)Polymers Exhibiting Tunable UCST Behavior in Water. *Macromol. Rapid Commun.* **2021**, 2100556.

(29) Lertturongchai, P.; Ibrahim, M. I. A.; Durand, A.; Sunintaboon, P.; Ferji, K. Synthesis of Thermoresponsive Copolymers with Tunable UCST-Type Phase Transition Using Aqueous Photo-RAFT Polymerization. *Macromol. Rapid Commun.* **2020**, No. 41, 2000058. https://doi.org/10.1002/marc.202000058.

(30) Zhao, C.; Ma, Z.; Zhu, X. X. Rational Design of Thermoresponsive Polymers in Aqueous Solutions: A Thermodynamics Map. *Progress in Polymer Science* **2019**, *90*, 269–291. https://doi.org/10.1016/j.progpolymsci.2019.01.001.

(31) Kim, Y.-J.; Matsunaga, Y. T. Thermo-Responsive Polymers and Their Application as Smart Biomaterials. *J. Mater. Chem. B* **2017**, *5* (23), 4307–4321. https://doi.org/10.1039/C7TB00157F.

(32) Bansal, K. K.; Upadhyay, P. K.; Saraogi, G. K.; Rosling, A.; Rosenholm, J. M. Advances in Thermo-Responsive Polymers Exhibiting Upper Critical Solution Temperature (UCST). *Express Polym. Lett.* **2019**, *13* (11), 974–992. https://doi.org/10.3144/expresspolymlett.2019.85.

(33) Roy, D.; Brooks, W. L. A.; Sumerlin, B. S. New Directions in Thermoresponsive Polymers. *Chem. Soc. Rev.* **2013**, *42* (17), 7214–7243. https://doi.org/10.1039/c3cs35499g.

(34) Seuring, J.; Agarwal, S. Polymers with Upper Critical Solution Temperature in Aqueous Solution. *Macromol. Rapid Commun.* **2012**, *33* (22), 1898–1920. https://doi.org/10.1002/marc.201200433.

(35) Seuring, J.; Agarwal, S. Polymers with Upper Critical Solution Temperature in Aqueous Solution: Unexpected Properties from Known Building Blocks. *ACS Macro Letters* **2013**, *2* (7), 597–600. https://doi.org/10.1021/mz400227y.

(36) Seuring, J.; Agarwal, S. First Example of a Universal and Cost-Effective Approach: Polymers with Tunable Upper Critical Solution Temperature in Water and Electrolyte Solution. *Macromolecules* **2012**, *45* (9), 3910–3918. https://doi.org/10.1021/ma300355k.

(37) Seuring, J.; Agarwal, S. Non-Ionic Homo- and Copolymers with H-Donor and H-Acceptor Units with an UCST in Water. *Macromol. Chem. Phys.* **2010**, *211* (19), 2109–2117. https://doi.org/10.1002/macp.201000147.

(38) Käfer, F.; Pretscher, M.; Agarwal, S. Tuning the Phase Transition from UCST-Type to LCST-Type by Composition Variation of Polymethacrylamide Polymers. *Macromol. Rapid Commun.* **2018**, *39* (24), 1800640. https://doi.org/10.1002/marc.201800640.

(39) Akiyama, Y. Synthesis of Temperature-Responsive Polymers Containing Piperidine Carboxamide and *N,N* -diethylcarbamoly Piperidine Moiety via RAFT Polymerization. *Macromol. Rapid Commun.* **2021**, *42* (15), 2100208. https://doi.org/10.1002/marc.202100208.

(40) Guinier, A. Small-Angle Scattering of X-Rays; New York, 1955; p 276.

(41) Pedersen, J. S. Analysis of Small-Angle Scattering Data from Colloids and Polymer Solutions: Modeling and Least-Squares Fitting I. *Adv. Colloid Interface Sci.* **1997**, *70*, 171–210.

(42) Fournet, G. Théorie de La Diffusion Des Rayons Par La Matière. *Bull. Soc. Fr. Mineral. Cristallogr.* **1951**, *74*, 39–113.

(43) McMillan, G. K.; Cameron, R. A. *Advanced PH Measurement and Control*; ISA, 2004.

(44) Biais, P.; Beaunier, P.; Stoffelbach, F.; Rieger, J. Loop-Stabilized BAB Triblock Copolymer Morphologies by PISA in Water. *Polymer Chemistry* **2018**, *9* (35), 4483–4491. https://doi.org/10.1039/C8PY00914G.

(45) Lacík, I.; Beuermann, S.; Buback, M. PLP−SEC Study into Free-Radical Propagation Rate of Nonionized Acrylic Acid in Aqueous Solution. *Macromolecules* **2003**, *36* (25), 9355–9363. https://doi.org/10.1021/ma030365e.

(46) Lacík, I.; Beuermann, S.; Buback, M. PLP-SEC Study into the Free-Radical Propagation Rate Coefficients of Partially and Fully Ionized Acrylic Acid in Aqueous Solution. *Macromol. Chem. Phys.* **2004**, *205* (8), 1080–1087. https://doi.org/10.1002/macp.200300251.

(47) Cabaness, W. R.; Lin, T. Y.-C.; Párkányi, C. Effect of PH on the Reactivity Ratios in the Copolymerization of Acrylic Acid and Acrylamide. *Journal of Polymer Science Part A-1: Polymer Chemistry* **1971**, *9* (8), 2155–2170. https://doi.org/10.1002/pol.1971.150090805.

(48) Thickett, S. C.; Gilbert, R. G. Propagation Rate Coefficient of Acrylic Acid: Theoretical Investigation of the Solvent Effect. *Polymer* **2004**, *45* (20), 6993–6999. https://doi.org/10.1016/j.polymer.2004.08.021.

(49) Slawinski, M.; Meuldijk, J.; Van Herk, A. M.; German, A. L. Seeded Emulsion Polymerization of Styrene: Incorporation of Acrylic Acid in Latex Products. *Journal of Applied Polymer Science* **2000**, *78* (4), 875–885. https://doi.org/10.1002/1097-4628(20001024)78:4<875::AID-APP220>3.0.CO;2-A.

(50) Byard, S. J.; Williams, M.; McKenzie, B. E.; Blanazs, A.; Armes, S. P. Preparation and Cross-Linking of All-Acrylamide Diblock Copolymer Nano-Objects via Polymerization-Induced Self-Assembly in Aqueous Solution. *Macromolecules* **2017**, *50* (4), 1482–1493. https://doi.org/10.1021/acs.macromol.6b02643.

(51) Wang, X.; Zhou, J.; Lv, X.; Zhang, B.; An, Z. Temperature-Induced Morphological Transitions of Poly(Dimethylacrylamide)–Poly(Diacetone Acrylamide) Block Copolymer Lamellae Synthesized via Aqueous Polymerization-Induced Self-Assembly. *Macromolecules* **2017**, *50* (18), 7222–7232. https://doi.org/10.1021/acs.macromol.7b01644.

(52) Otsuka, C.; Wakahara, Y.; Okabe, K.; Sakata, J.; Okuyama, M.; Hayashi, A.; Tokuyama, H.; Uchiyama, S. Fluorescent Labeling Method Re-Evaluates the Intriguing Thermoresponsive Behavior of Poly(Acrylamide- *Co* -Acrylonitrile)s with Upper Critical Solution Temperatures. *Macromolecules* **2019**, *52* (20), 7646–7660. https://doi.org/10.1021/acs.macromol.9b00880.

(53) Käfer, F.; Liu, F.; Stahlschmidt, U.; Jérôme, V.; Freitag, R.; Karg, M.; Agarwal, S. LCST and UCST in One: Double Thermoresponsive Behavior of Block Copolymers of Poly(Ethylene Glycol) and Poly(Acrylamide -*Co*- Acrylonitrile). *Langmuir* **2015**, *31* (32), 8940–8946. https://doi.org/10.1021/acs.langmuir.5b02006.